UNIFIED SURGICAL WORLD MODEL FOR STRUCTURED UNDERSTANDING, LONG-HORIZON PREDICTION, AND FINE-GRAINED GENERATION

Anonymous authors
Paper under double-blind review

ABSTRACT

World models are capable of learning environment dynamics and supporting long-horizon prediction and data-efficient policy learning by synthesizing plausible rollouts. These models provide a flexible and powerful framework for training agents in environments where data is scarce, annotation is costly, and exploration is constrained. In the context of surgery, the surgical intelligence field faces significant challenges due to the lack of high-quality and diverse multimodal data for training surgical vision-language models, as well as the absence of highly realistic simulators for training surgical robots. Surgical world models address these challenges by both generating multimodal data and serving as a surgical embodied simulator, making them ideal for advancing surgical robotics and intelligence. We propose a Unified Surgical World Model (UniSWM), which unifies structured understanding, long-horizon prediction, and fine-grained generation through a mixture of transformers. UniSWM acts as both a data generator and a simulator for surgical robotics, supporting vision–language and vision–language–action training across in-body and operating room settings. This model integrates structured understanding with discrete action tokens for phase, step, action, and movement, and supports long-horizon prediction for multi-step surgical trajectories. It conditions fine-grained generation on action and movement tokens, aligning frames to deterministic textual descriptions, and eliminates the need for optical flow or kinematic labels. To enable the training of world models, we introduce UniSWM-DB, a diverse multimodal dataset containing 1.81 million samples specifically designed for surgical training. To evaluate the capabilities of UniSWM, we propose UniSWM-Bench, a comprehensive benchmark covering five understanding tasks, two prediction tasks, and three generation tasks. Experimental results demonstrate that UniSWM significantly outperforms existing models, including GPT-5, Gemini-2.5-Pro, and Qwen-VL-Max, excelling in structured understanding, long-horizon prediction, and coherent, controllable visual generation.

1 INTRODUCTION

World models provide a powerful framework for learning environment dynamics (Li et al., 2025; Zhao et al., 2025a), supporting long-horizon prediction, and enabling data-efficient policy learning by synthesizing plausible rollouts (Ha & Schmidhuber, 2018; Hafner et al., 2019). These capabilities are especially valuable in domains where data is scarce, annotation is costly, and exploration is restricted (Xiang et al., 2023; Ding et al., 2024b). In the context of surgery, the field of surgical intelligence faces significant challenges due to the lack of high-quality, diverse multimodal data necessary for training surgical vision-language models (VLMs), as well as the absence of highly realistic simulators for training surgical robots (Zeng et al., 2025b; Min et al., 2025). Surgical world models address these challenges by both generating multimodal data and serving as an embodied simulator for surgical robotics, enabling realistic and data-efficient training for both VLMs and vision-language-action (VLA) models (Zhao et al., 2025b; Lu et al., 2025).

Despite advances in surgical scene analysis and generative modeling (Khan et al., 2025), current systems remain fragmented, often focusing on isolated tasks such as phase recognition, action prediction, or single-view video generation (Hamoud et al., 2025; Schmidt et al., 2021). These approaches typically concentrate on in-body videos and fail to provide mechanisms for predicting future states or controlling instrument behavior (Twinanda et al., 2017; Jin et al., 2021; Ho et al., 2020; Rombach et al., 2022; Cho et al., 2024; Iliash et al., 2024; CAMMA Lab). As a result, they lack the capability to comprehensively model surgical workflows and to generate realistic, controllable simulations for surgical robots.

To address these limitations, we propose a Unified Surgical World Model (UniSWM), a framework that unifies structured understanding, long-horizon prediction, and fine-grained generation through a mixture of transformers. It serves dual roles as both a data generator and a simulator for surgical robotics, supporting vision–language and vision–language–action training across in-body and operating room (OR) settings (Paik et al., 2014). UniSWM organizes control using discrete *action tokens*, which capture structured aspects of the surgical workflow. Furthermore, it enables long-horizon prediction by forecasting multi-step Phase and Step trajectories, and supports fine-grained generation conditioned on action and movement tokens. This capability allows UniSWM to produce realistic and coherent visual outputs that evolve according to the surgical context.

To enable the training of world models, we introduce UniSWM-DB, a diverse multimodal dataset containing 1.81 million samples specifically designed for surgical training. We also propose UniSWM-Bench, a comprehensive benchmark covering five understanding tasks, two prediction tasks, and three generation tasks, which allows us to evaluate the model's performance in recognition, controllable synthesis, and long-horizon forecasting within a unified framework.

Our contributions are fivefold:

1. We present UniSWM, a unified surgical world model that integrates structured understanding, long-horizon prediction, and fine-grained generation across in-body and OR scenes.
2. We implement structured understanding through discrete action tokens, which capture the hierarchical aspects of the surgical workflow, enabling effective structured scene analysis.
3. We enable long-horizon prediction by forecasting multi-step Phase and Step trajectories, planning in latent space, and advancing the latent state under predicted actions and movements, decoding boundary frames only when necessary to preserve global coherence.
4. We achieve fine-grained, token-driven generation by conditioning on action and movement tokens, aligning generated frames with deterministic textual descriptions.
5. We propose UniSWM-DB, a diverse multimodal dataset containing 1.81 million samples for training surgical world models, and UniSWM-Bench, a comprehensive evaluation suite covering five understanding tasks, two prediction tasks, and three generation tasks.

2 RELATED WORK

World model World model learn latent dynamics for imagination-based control, long-horizon forecasting, and data efficiency (Ha & Schmidhuber, 2018; Hafner et al., 2019). Subsequent advances combine stochastic latent rollouts with value learning to stabilize training and improve sample efficiency (Hafner et al., 2019). In parallel, diffusion and latent diffusion substantially improved fidelity and temporal coherence in forward prediction and synthesis (Ho et al., 2020; Rombach et al., 2022; Cao et al., 2024). Vision–language–action (VLA) systems further connect internet-scale knowledge with embodied policies (Ma et al., 2024; Brohan et al., 2023; Driess et al., 2023; Kim et al., 2025). UniSWM situates itself at this intersection by unifying understanding, controllable generation, and long-horizon prediction under a single, domain-tailored framework.

Surgical Intelligence Surgical perception has progressed across phase recognition, tool analysis, and workflow modeling (Demir et al., 2023; Ding et al., 2024a), with canonical efforts in endoscopic phase recognition and video modeling (Twinanda et al., 2017; Jin et al., 2021; CAMMA Lab). Community benchmarks expanded evaluation to OR context and instrument segmentation (Escamirosa et al., 2015; Allan et al., 2019; Srivastav et al., 2018), yet joint modeling of in-body and OR signals with forward prediction remains limited. Diffusion-based generation is emerging for surgical content creation and interactive synthesis (Cho et al., 2024; Iliash et al., 2024; Zeng et al., 2025a), but action/movement–conditioned futures that preserve instrument kinematics and tissue realism are underexplored.

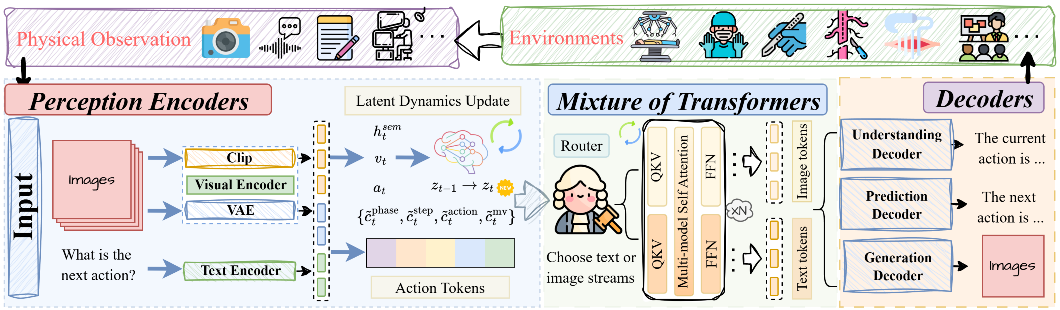

Figure 1: Overview of UniSWM, showing the end-to-end pipeline from multimodal perception to structured understanding, long-horizon prediction, and fine-grained generation.

3 METHOD

3.1 OVERVIEW

UniSWM encodes multimodal observations into a compact latent state, advances this state under a set of action tokens that reflect the surgical hierarchy, and decodes both future states and visuals using a decoder-only foundation model conditioned on specific tokens from the text prompt. The model performs structured understanding, long-horizon prediction, and fine-grained generation. As depicted in Figure 2, the **Left** part demonstrates latent dynamics involving visual, text, and action tokens across Phase, Step, Atomic Action, and Movement. Meanwhile, the **Middle** part presents the foundation of MoT (Mixture of Transformers), which selects the optimal corresponding streams for each task. Moreover, the **Right** part showcases three distinct decoders for the purposes of understanding, prediction, and generation. In the following, we illustrate each module of our model in detail.

Initial Scene Generation Before the pipeline begins, the model initializes the scene from a textual prompt: we apply $\mathrm{Tok}(u_0) \xrightarrow{\text{MoT}} \hat{u}_0 \xrightarrow{\text{Dec}_{\text{gen}}}$ Initial Scene. This optional step provides a coherent visual state for subsequent reasoning and synthesis.

Perception Encoders Perception supplies semantically aligned *vision features* for understanding and high-fidelity *latents* for generation. We denote visual observations by x_t and text instructions by u_t. Two complementary encoders are used: a CLIP-style semantic encoder and a VAE-style generative encoder. The CLIP-style semantic encoder maps images and project the image embedding into a sequence of visual tokens consumed by the LLM: $e_t^{\text{img}} = \mathrm{Enc}_{\text{img}}(x_t),\ s_t^{\text{vis}} = \mathrm{Tok}_{\text{vis}}\big(e_t^{\text{img}}\big)$. The VAE-style generative encoder compresses frames into latents suitable for high-fidelity synthesis: $v_t = \mathrm{Enc}_{\text{gen}}(x_t),\ \hat{x}_t = \mathrm{Dec}_{\text{vae}}(v_t)$.

Latent Dynamics and Action Tokens A recurrent latent aggregates recent evidence and provides a substrate for imagination: $z_t \sim p_\phi\big(z_t \,\big|\, z_{t-1},\, s_t^{\text{vis}},\, v_t,\, a_{t-1}\big)$. Surgical control is expressed with four discrete token sequences mirroring clinical hierarchy: Phase and Step capture workflow progression; Atomic Action describes intended instrument usage; Movement captures short-horizon motion primitives via a vector-quantized codebook over motion patterns: $\tilde{c}_t = \big\{\tilde{c}_t^{\text{phase}},\ \tilde{c}_t^{\text{step}},\ \tilde{c}_t^{\text{action}},\ \tilde{c}_t^{\text{mv}}\big\}$.

Foundation with Mixture of Transformers We instantiate the foundation model for long-horizon prediction and fine-grained generation using a Mixture-of-Transformers (MoT) architecture. First, a shared multi-modal stem computes contextualized hidden states for the entire serialized context: $H_t^{(0)} = \mathrm{Stem}_\theta(\mathcal{C}_t,\, z_t)$, where Stem_θ is a stack of self-attention and MLP blocks with unified positional encoding for all token types. After this, two *full Transformer branches* specialize the representation for language understanding/planning and visual planning respectively: $H_t^{\text{und}} = \mathrm{Transf}_{\psi_{\text{und}}}\Big(H_t^{(0)}\Big), \qquad H_t^{\text{gen}} = \mathrm{Transf}_{\psi_{\text{gen}}}\Big(H_t^{(0)}\Big)$. A lightweight router then produces mixture weights for text and image streams (or selects a top-1 branch). With a pooled summary $\mathrm{Pool}(H_t^{(0)})$, we compute

$$\alpha^{\text{text}} = \mathrm{Softmax}\big(W_{\mathrm{r}}^{\text{text}} \cdot \mathrm{Pool}(H_t^{(0)})\big), \quad \alpha^{\text{img}} = \mathrm{Softmax}\big(W_{\mathrm{r}}^{\text{img}} \cdot \mathrm{Pool}(H_t^{(0)})\big) \in \mathbb{R}^2.$$

The branch-specific hidden states for each stream are

$$\bar{H}_t^{\text{text}} = \alpha_1^{\text{text}} H_t^{\mathrm{und}} + \alpha_2^{\text{text}} H_t^{\mathrm{gen}}, \qquad \bar{H}_t^{\text{img}} = \alpha_1^{\text{img}} H_t^{\mathrm{und}} + \alpha_2^{\text{img}} H_t^{\mathrm{gen}}.$$

Finally, separate vocabularies/Codebooks decode the two streams in *one forward pass*:

$$F_\theta^{\text{text}}(\mathcal{C}_t, z_t) = \mathrm{AR}\big(\mathrm{Softmax}(W_{\text{text}} \bar{H}_t^{\text{text}})\big), \qquad F_\theta^{\text{image}}(\mathcal{C}_t, z_t) = \mathrm{AR}\big(\mathrm{Softmax}(W_{\text{img}} \bar{H}_t^{\text{img}})\big).$$

"interleaved" refer to serializing the two streams into one sequence with sentinel tags, $\langle\texttt{TEXT}\rangle\, \hat{s}\, \langle/\texttt{TEXT}\rangle\ \langle\texttt{IMG}\rangle\, \hat{u}\, \langle/\texttt{IMG}\rangle$, while routing ensures each segment predominantly uses its appropriate branch. At test time, decoding proceeds in a single pass with shared KV-cache: (a) generate the text stream (greedy or nucleus sampling) until <EOS_TEXT>; (b) generate the image/clip planning tokens until <EOS_IMG>. Both streams reuse the stem states and differ only in the routed branch and output vocabulary. There is no speculative multi-pass decoding or latent rollout here, and the produced text tokens or visual tokens are then consumed by the understanding decoder, prediction decoder and generation decoder.

Understanding Decoder for Structured Scene Analysis We reinterpret near-term text tokens to estimate the current surgical state. At time t, the understanding decoder produces *six* textual heads: phase, step, action, triplet, grounding, and environment. Each head is a short token sequence generated under teacher forcing:

$$\big(\hat{s}_t^{\mathrm{phase}},\, \hat{s}_t^{\mathrm{step}},\, \hat{s}_t^{\mathrm{action}},\, \hat{s}_t^{\mathrm{trip}},\, \hat{s}_t^{\mathrm{grd}},\, \hat{s}_t^{\mathrm{env}}\big) \;=\; \mathrm{Dec}_{\mathrm{und}}\big(\hat{s}_t\big). \tag{1}$$

Here, *Phase* is the workflow stage, *Step* refines the phase, *Action* denotes the atomic operation, and *Triplet* consists of "(instrument,verb ,target)". On the other hand, *Grounding* outputs $[x_1, y_1, x_2, y_2] \in [0,1]^4$ (optionally quantized), and *Environment* briefly describes residual factors (e.g., visibility, bleeding). The target strings are $s_t^{\mathrm{phase}}, s_t^{\mathrm{step}}, s_t^{\mathrm{action}}, s_t^{\mathrm{trip}}, s_t^{\mathrm{grd}}, s_t^{\mathrm{env}}$. With tokenizer $\mathrm{Tok}(\cdot)$ and vocabulary $\mathcal{V}$, we train the understanding decoder with token-level cross-entropy:

$$\mathcal{L}_{\mathrm{und}} = \sum_{h \in \{\mathrm{phase,step,action,trip,grd,env}\}} \sum_{\ell=1}^{L_h} \mathrm{CE}\Big(w_\ell^{(h)},\, \hat{p}_\ell^{(h)}\Big(\cdot \mid w_{<\ell}^{(h)}\Big)\Big). \tag{2}$$

Prediction Decoder for Long-horizon States Given the current latent z_t and the textual summaries, the prediction decoder generates a horizon of workflow states as text. Formally, it's conditioned on z_t, $\hat{s}_t^{\mathrm{phase}}$, and $\hat{s}_t^{\mathrm{step}}$, then outputs two serialized sequences for $[t{+}1,\, t{+}H]$:

$$\big(\hat{s}_{t+1:t+H}^{\mathrm{phase}},\, \hat{s}_{t+1:t+H}^{\mathrm{step}}\big) \;=\; \mathrm{Dec}_{\mathrm{pred}}\big(z_t,\, \hat{s}_t^{\mathrm{phase}},\, \hat{s}_t^{\mathrm{step}}\big). \tag{3}$$

Denote the ground-truth strings by $s_{t+1:t+H}^{\mathrm{phase}}$ and $s_{t+1:t+H}^{\mathrm{step}}$, training of the prediction decoder uses token-level cross-entropy over the serialized horizons.

Generation Decoder for Fine-grained Visuals The generation decoder synthesizes a *single* target frame at a specified look-ahead k using only information available at time t. The design choice of the generation decoder can be quite flexible, and in this article, we apply the latent diffusion (flow) based method, which consists of a conditional generation model and an auto-encoder. More precisely, the generation process is controlled by z_t, on image-side planning tokens $\hat{u}_{t+\Delta k}$ predicted at time t, and on planned control tokens $\tilde{c}_{t+\Delta k}^{\mathrm{action}}$ and $\tilde{c}_{t+\Delta k}^{\mathrm{mv}}$:

$$\hat{v}_{t+\Delta k} \sim \mathrm{Dec}_{\mathrm{gen}}\big(z_t,\, \hat{u}_{t+\Delta k},\, \tilde{c}_{t+\Delta k}^{\mathrm{action}},\, \tilde{c}_{t+\Delta k}^{\mathrm{mv}}\big), \qquad \hat{x}_{t+\Delta k} = \mathrm{Dec}_{\mathrm{vae}}\big(\hat{v}_{t+\Delta k}\big), \tag{4}$$

for $\Delta k \in \{1, \ldots, H\}$. Note that there is no autoregressive rollout over future frames: each $\hat{x}_{t+\Delta k}$ is generated directly from the context at time t. For training, the visual generation loss (denoted by $\mathcal{L}_{\text{gen}}$), corresponds to the standard flow matching loss.

Training Objective The final objective aggregates all the components defined above: understanding, prediction, and generation:

$$\mathcal{L} = \gamma\, \mathcal{L}_{\text{und}} + \alpha\, \mathcal{L}_{\text{pred}} + \beta\, \mathcal{L}_{\text{gen}},$$

where $\mathcal{L}_{\text{und}}$, $\mathcal{L}_{\text{pred}}$, and $\mathcal{L}_{\text{gen}}$ are the losses for understanding, prediction, and generation, respectively.

4 Experiments

Dataset We evaluate the performance of the UniSWM model using the UniSWM-DB dataset, a comprehensive multimodal dataset designed to support the training and evaluation of models in the context of surgical intelligence. As shown in Figure 1, the dataset consists of a variety of tasks across three main categories: Generation, Prediction, and Understanding. Specifically, it includes tasks such as Caption Control (Out-of-body), Movement & Action Control (In-body), Phase Prediction (In-body), Step Prediction (In-body), as well as various Understanding tasks like Action Recognition, Caption Generation, Safety Recognition, and Visual Question Answering, among others. The dataset contains a total of over 1.81 million samples, with each task and sub-task having its own distinct distribution and data partitioning.

Benchmark UniSWM-Bench serves as the evaluation benchmark for UniSWM and includes a task distribution designed to test the model's ability to handle a wide range of surgical tasks. The benchmark is divided into three major categories: Understanding (5 Tasks), Prediction (2 Tasks), and Generation (3 Tasks). As shown in Table 2, tasks within the Understanding category include Phase Recognition, Action Recognition, Triplet Recognition, Instrument Grounding, and Environment Recognition, with sample sizes ranging from 0.5K to 1K per task. The Prediction category includes Phase Prediction and Step Prediction, with 4K samples per task. For the Generation category, the benchmark evaluates Scene Initialization and Scene Evolution, both with 0.5K samples each. These tasks span both in-body and out-of-body surgical contexts and are critical for assessing the model's performance in terms of both real-time understanding and long-horizon predictions.

Table 1: UniSWM-DB task distribution.

Type	Task & Generation Condition	Domain	Count
Generation	Caption Control	Out-of-body	109K
Generation	Movement & Action Control	In-body	171K
Prediction	Phase Prediction	In-body	40K
Prediction	Step Prediction	In-body	40K
Understanding	Action Recognition	In-body	390K
Understanding	Caption Generation	Out-of-body	164K
Understanding	Caption Generation	In-body	306K
Understanding	Phase Recognition	In-body	311K
Understanding	Safety Recognition	In-body	110K
Understanding	Triplet Recognition	In-body	103K
Understanding	Visual Question Answering	In-body	11K

Table 2: UniSWM-Bench task distribution.

Type	Domain	Task	Count
Understanding	In-body	Phase Recognition	1K
	In-body	Action Recognition	1K
	In-body	Triplet Recognition	1K
	In-body	Instrument Grounding	1K
	In-body	Environment Recognition	0.5K
Prediction	In-body	Phase Prediction	4K
	In-body	Step Prediction	4K
Generation	In-body	Scene Initialization	0.5K
	In-body	Scene Evolution	0.5K
	Out-of-body	Scene Initialization	0.5K

4.1 Evaluation of Structured Understanding

In this evaluation, we compare a total of 29 models, including open-source variants, and conduct stability tests (see Appendix for details). However, the main comparison focuses on two strong general-purpose Vision-Language Models (VLMs), Gemini-2.5-Pro and GPT-5, using the UniSWM-Bench protocol across various tasks. These tasks assess the model's ability to understand and process structured understanding of the surgical workflow, including workflow recognition, compositional semantics recognition, spatial perception, and environment answering (see Table 3).

Workflow Recognition The first crucial step in structured understanding is workflow recognition, which involves recognizing phases and actions within the surgical procedure. General VLMs show moderate performance on this task, with GPT-5 achieving accuracy, precision, recall, and Jaccard scores of 28.30/0.65/0.70/7.18, and Gemini-2.5-Pro showing 28.30/16.23/13.95/6.06. These models struggle with the finer nuances of phase transitions and action timings due to their reliance on instruction-following mechanisms without deeper temporal reasoning. UniSWM, by contrast, leverages latent dynamics with action-aware conditioning, achieving 81.90/71.79/67.59/54.42 on phase

Table 3: Evaluation of structured understanding on UniSWM-Bench across five tasks.

Model	Phase Recognition				Action Recognition				Triplet Recognition				Instrument Grounding				Environment Answering			
	Acc.	Pre.	Rec.	Jac.	Acc.	Pre.	Rec.	Jac.	Acc.	Ins.	Ver.	Tar.	mIoU	mAP$_{50}$	mAP$_{75}$	AP	Acc.	B4	MET	R1
SmolVLM2-2.2B	20.81	12.18	15.37	6.35	14.93	13.05	12.25	5.61	0.00	7.87	3.71	0.62	2.89	0.27	0.07	0.08	23.65	3.03	12.19	15.60
Skywork-R1V-38B	6.94	17.24	14.31	1.56	11.83	14.42	12.62	2.76	0.12	21.06	9.33	2.25	9.86	1.60	0.00	0.28	35.63	0.32	1.36	1.56
Phi4-Multimodal	17.92	14.14	15.50	5.36	24.37	13.35	12.38	5.74	0.29	11.50	12.58	3.87	1.17	0.13	0.00	0.04	34.25	0.34	1.48	1.74
Mistral-Small-24B	25.60	26.80	25.92	11.64	12.50	5.73	12.68	1.78	0.50	9.08	8.79	5.96	17.64	5.93	0.27	1.45	36.79	0.15	0.59	0.71
PaliGemma2-3B	7.29	10.08	13.90	2.35	11.57	13.92	12.58	2.26	0.00	0.96	2.19	3.06	0.01	0.00	0.00	0.00	31.78	1.55	5.65	9.04
Llama-4-Scout-17B-16E	40.70	27.96	18.02	8.71	30.97	19.46	12.75	4.66	0.21	3.35	3.56	7.46	36.72	35.73	7.17	12.99	36.99	0.04	0.20	0.33
Kimi-VL-A3B-Instruct	35.00	20.79	19.04	10.25	25.23	12.10	14.17	6.91	0.02	12.04	9.83	2.14	9.63	4.93	0.73	1.62	32.11	1.65	6.62	8.60
Kimi-VL-A3B-Thinking	6.53	16.61	14.31	1.06	11.23	14.07	12.90	2.33	0.04	6.50	9.21	1.08	9.36	1.90	0.13	0.48	34.09	0.34	1.44	1.74
Gemma3-27B	14.03	25.37	16.93	4.52	31.97	20.60	13.50	5.01	0.13	10.00	6.35	1.67	17.45	6.17	0.10	1.41	36.02	0.03	0.13	0.26
MiMo-VL-7B-SFT	20.90	20.73	16.46	7.15	24.37	17.56	15.72	7.40	0.13	7.98	5.10	4.85	33.45	28.57	2.80	8.55	35.40	0.09	0.37	0.66
MiMo-VL-7B-RL	25.73	15.73	14.77	6.77	26.90	14.21	14.04	7.05	0.21	6.25	5.14	2.14	36.86	34.77	3.77	10.78	34.97	0.10	0.40	0.74
MiniCPM-V-2_6	16.85	14.24	14.20	6.10	24.43	14.14	13.42	7.41	0.04	17.02	13.93	1.35	17.87	7.33	0.57	1.87	33.32	1.14	5.50	6.18
MiniCPM-o-2_6	15.10	23.77	20.63	8.68	29.67	12.60	12.47	5.22	0.35	23.31	8.92	5.29	20.33	9.80	1.10	2.96	35.29	0.24	0.74	1.15
Qwen-Omni-3B	34.16	18.11	18.27	10.59	28.23	12.76	12.38	5.69	0.00	10.33	7.06	1.31	22.17	16.20	3.47	6.25	35.03	0.14	0.87	0.73
Qwen-Omni-7B	22.01	18.16	18.10	7.66	29.93	29.58	13.20	5.81	0.15	10.79	6.87	5.46	34.60	40.53	5.63	14.17	37.45	0.26	1.06	1.24
Qwen2.5-VL-7B	27.57	20.50	18.48	8.33	31.17	5.82	12.55	4.02	0.23	9.92	4.65	5.21	10.63	0.97	0.03	0.26	37.17	4.43	15.14	13.27
Qwen2.5-VL-32B	44.77	26.83	22.05	13.63	31.67	31.84	13.72	5.34	0.23	26.22	6.69	2.10	11.36	1.93	1.07	1.03	42.43	0.21	2.08	1.74
Qwen2.5-VL-72B	37.03	23.75	20.21	10.82	28.83	16.52	13.42	6.21	0.19	26.33	8.16	4.58	42.70	45.95	25.75	25.69	41.89	0.24	1.62	2.37
InternVL3-8B	30.93	22.21	19.38	10.71	29.30	14.16	13.03	6.36	1.65	51.49	8.87	24.39	22.49	7.13	0.20	1.58	34.77	0.98	4.37	4.35
InternVL3-78B	33.17	34.01	25.25	15.05	28.77	21.24	12.69	6.22	0.37	37.39	8.54	3.44	29.41	18.20	1.60	4.99	36.70	0.16	1.39	0.92
MedVLM-R1	10.50	12.54	16.15	2.40	31.13	16.39	12.52	3.94	0.02	45.72	8.98	0.31	5.31	0.30	0.00	0.03	31.25	2.42	7.66	10.85
Lingshu-7B	39.77	13.63	23.53	9.07	31.50	16.41	12.92	4.33	0.08	2.15	7.98	3.65	28.72	26.13	3.37	8.20	35.41	0.71	2.74	3.02
Lingshu-32B	36.31	23.98	22.22	12.85	26.60	20.07	17.96	10.09	0.21	21.04	7.17	3.77	26.03	18.20	2.90	5.89	34.69	0.11	0.59	0.74
MedGemma-4B	27.07	18.53	23.33	9.63	22.50	4.42	12.32	3.53	0.00	2.89	8.17	1.42	9.43	0.57	0.00	0.08	37.09	0.05	0.32	0.58
MedGemma-27B	43.40	24.68	15.30	7.37	29.90	20.73	12.38	4.73	0.13	8.39	3.65	3.62	17.20	2.23	0.00	0.44	35.98	0.05	0.24	0.44
SurgVLM-72B	73.05	64.91	65.30	49.10	45.13	30.05	31.88	18.60	4.91	47.66	12.91	38.91	59.34	74.20	28.30	36.28	69.52	46.65	58.16	74.58
Qwen-VL-Max-Latest	43.40	6.20	14.29	6.20	24.90	9.38	11.95	6.04	2.32	75.53	9.18	71.84	8.53	0.30	0.00	0.05	34.50	0.64	0.53	0.64
GPT-5-0807-Global	28.30	0.65	0.70	7.18	14.20	6.36	8.00	2.79	1.90	54.85	9.28	44.83	1.92	1.20	0.40	0.50	36.98	1.72	1.61	1.72
Gemini-2.5-Pro-06-17	28.30	16.23	13.95	6.06	25.60	9.34	12.21	4.94	0.00	45.06	34.24	8.20	27.92	15.90	1.60	4.90	34.37	2.44	2.08	2.44
UniSWM	**81.90**	**71.79**	**67.59**	**54.42**	**63.40**	**57.44**	**42.77**	**31.34**	**47.51**	**71.81**	**64.56**	**49.77**	**88.11**	**94.20**	**88.70**	**73.75**	**69.85**	**92.83**	**97.24**	**94.17**

recognition and 63.40/57.44/42.77/31.34 on action recognition. The significant performance improvement emphasizes the importance of structured understanding for temporal modeling in surgical workflows, which general VLMs cannot fully capture.

Compositional Semantics Recognition The ability to reason compositely over instruments, verbs, and targets is essential for understanding the context of a surgical procedure. General VLMs such as GPT-5 achieve only 1.90% triplet accuracy, with factor-wise scores of 54.85/9.28/44.83 for instrument/verb/target, while Gemini-2.5-Pro yields 0.00% accuracy and factor-wise scores of 45.06/34.24/8.20. This indicates that these models struggle with maintaining global consistency across the components of surgical actions. UniSWM significantly improves on this by achieving 47.51% triplet accuracy and enhancing factor-wise scores to 71.81/64.56/49.77. The discrepancy between the factor-wise and joint triplet scores in general VLMs highlights their weak semantic coherence. UniSWM's structured approach enforces compatibility among participants (instruments), predicates (verbs), and entities (targets), providing a more integrated and semantically consistent understanding of the surgical action.

Spatial Perception Accurate spatial perception is essential in surgery, particularly for tasks such as instrument localization and environment interaction. For instrument grounding, GPT-5 achieves only 1.92 mIoU, 1.20 mAP$_{50}$, 0.40 mAP$_{75}$, and 0.50 AP. Gemini-2.5-Pro fares slightly better with 27.92 mIoU, 15.90 mAP$_{50}$, 1.60 mAP$_{75}$, and 4.90 AP. However, UniSWM outperforms both with substantial margins, reaching 88.11 mIoU, 94.20 mAP$_{50}$, 88.70 mAP$_{75}$, and 73.75 AP. These results reveal that traditional VLMs, which are designed for generic visual question answering, fail to handle the dense spatial localization required in surgical tasks. UniSWM's approach ties temporal states with spatial entities, resulting in more consistent and accurate pixel-level predictions that align with the complex spatial relationships in the operating room.

Environment Answering Finally, environment answering assesses the model's ability to generate coherent, linguistically rich responses based on the surgical scene. General VLMs show moderate recognition accuracy but poor language quality. GPT-5 achieves 36.98% accuracy, with BLEU-4 of 1.72, METEOR of 1.61, and ROUGE-1 of 1.72, while Gemini-2.5-Pro performs slightly better with 34.37% accuracy and BLEU-4 of 2.44. However, both models struggle to generate fluent and accurate responses due to their focus on either recognition or language quality, but not both. UniSWM, by contrast, achieves 69.85% accuracy, with significantly higher language generation metrics: BLEU-4 of 92.83, METEOR of 97.24, and ROUGE-1 of 94.17. This demonstrates that

UniSWM not only recognizes the environmental context accurately but also generates linguistically coherent responses, effectively closing the loop of structured understanding by ensuring that the perceived scene and the language generated are both faithful to the task and its context.

Table 4: Long-horizon prediction evaluation in UniSWM-Bench. H indicates the horizon between current time and target timestamp. Top: comparison with models trained on UniSWM-DB. Bottom: comparison with mainstream commercial models.

Model	H = 1s					H = 5s					H = 30s					H = 60s				
	Acc.	Pre.	Rec.	F1	Jac.	Acc.	Pre.	Rec.	F1	Jac.	Acc.	Pre.	Rec.	F1	Jac.	Acc.	Pre.	Rec.	F1	Jac.
Phase																				
InternVL3-8B	18.30	12.09	10.84	10.44	5.79	20.80	14.25	14.13	12.98	7.47	21.10	13.33	14.23	12.89	7.31	26.50	20.40	18.87	18.54	10.80
Gemma-3-27B	9.90	8.90	9.60	7.71	4.10	9.20	6.70	9.32	7.54	3.99	9.10	6.54	8.90	7.19	3.81	8.60	15.32	8.84	7.42	3.92
Gemma3-4B	21.00	17.87	12.34	11.14	6.30	22.60	13.42	12.20	10.66	6.04	20.40	8.51	10.49	8.57	4.83	23.40	11.67	9.21	9.05	5.13
Qwen2.5-VL-7B	20.50	13.17	14.41	13.04	7.42	19.90	14.41	15.14	13.48	7.64	17.80	14.88	12.65	12.29	6.86	20.30	16.05	15.22	14.47	8.04
LLaVA1.5-7B	20.00	12.64	13.18	11.55	6.51	16.80	10.63	11.01	9.49	5.23	20.20	17.29	11.40	9.93	5.53	24.20	19.50	14.46	14.39	8.16
SurgVLM-7B	18.10	19.24	11.90	9.50	5.35	16.00	13.21	12.85	11.77	6.51	19.80	18.42	15.09	13.77	7.69	18.10	14.79	13.97	13.66	7.55
UniSWM	**63.20**	**76.10**	**69.14**	**66.84**	**54.81**	**65.60**	**71.02**	**72.58**	**66.54**	**52.56**	**52.80**	**60.06**	**63.02**	**58.11**	**42.65**	**56.80**	**58.58**	**54.19**	**52.16**	**39.74**
Step																				
InternVL3-8B	17.50	8.83	7.06	6.84	3.74	18.60	8.20	9.17	8.08	4.47	18.40	4.57	6.18	5.04	2.84	22.30	10.93	10.65	9.41	5.29
Gemma-3-27B	5.70	4.82	2.67	1.92	1.01	6.90	2.13	2.53	2.00	1.07	7.20	1.92	3.26	2.08	1.10	5.50	1.82	1.93	1.42	0.75
Gemma3-4B	19.80	13.04	8.20	7.71	4.27	20.30	7.97	6.53	6.07	3.38	20.10	5.50	6.02	5.14	2.88	22.60	9.30	7.28	7.20	4.05
Qwen2.5-VL-7B	20.30	8.27	9.23	8.35	4.71	16.40	7.90	7.94	7.20	3.96	18.20	7.62	7.99	7.09	3.93	18.40	7.64	8.25	7.23	4.00
LLaVA1.5-7B	17.10	7.26	6.41	6.14	3.41	16.60	4.16	5.38	4.55	2.54	20.60	8.19	6.07	5.31	3.01	23.70	7.72	8.46	7.65	4.38
SurgVLM-7B	18.90	8.49	4.85	4.26	2.40	15.70	7.89	6.16	5.84	3.18	17.60	8.43	5.96	5.32	2.92	18.10	5.25	6.10	5.26	2.91
UniSWM	**49.60**	**23.64**	**31.50**	**24.25**	**19.02**	**52.00**	**23.00**	**42.97**	**28.35**	**20.92**	**64.80**	**30.51**	**39.30**	**30.08**	**25.25**	**55.20**	**30.09**	**41.56**	**31.37**	**25.39**
Phase&Step																				
InternVL3-8B	13.60	3.61	3.42	2.91	1.58	13.80	3.48	3.93	3.25	1.78	14.40	2.11	3.69	2.34	1.30	16.70	6.01	5.26	4.73	2.61
Gemma-3-27B	1.80	2.66	2.75	1.23	0.65	2.00	1.06	1.13	0.93	0.48	2.00	0.80	1.54	0.86	0.44	1.60	0.88	0.52	0.50	0.26
Gemma3-4B	15.50	6.31	3.73	3.26	1.78	17.60	4.87	2.71	2.31	1.28	17.90	3.04	3.01	2.37	1.31	18.00	3.37	3.50	3.14	1.74
Qwen2.5-VL-7B	14.00	3.61	4.29	3.58	1.97	12.00	3.32	3.69	2.90	1.57	13.50	3.92	4.02	3.51	1.92	13.20	4.48	4.71	3.83	2.07
LLaVA1.5-7B	13.60	3.75	3.34	3.03	1.67	12.20	2.07	2.38	1.81	0.99	17.00	4.17	2.77	2.39	1.32	18.10	4.61	3.90	3.64	2.04
SurgVLM-7B	12.90	3.74	2.85	1.66	0.93	10.60	4.69	2.80	2.77	1.49	12.80	4.03	3.39	2.56	1.37	10.90	2.99	2.98	2.56	1.37
UniSWM	**31.00**	**10.19**	**9.44**	**8.49**	**5.97**	**36.60**	**13.42**	**12.31**	**10.67**	**7.57**	**35.40**	**9.97**	**10.59**	**9.34**	**6.62**	**33.30**	**11.67**	**9.78**	**8.43**	**5.79**
Phase																				
Qwen-VL-Max	44.72	33.83	32.79	31.11	24.89	51.20	34.97	31.39	30.67	24.54	55.74	40.58	44.12	39.71	31.77	41.80	31.37	35.10	31.96	25.56
GPT-5	52.42	29.14	38.46	32.94	26.35	51.64	25.65	34.81	29.06	23.24	55.65	26.74	37.11	30.22	24.18	39.84	21.81	35.07	26.00	20.80
Gemini-2.5-Pro	39.52	23.81	38.27	25.65	20.52	43.20	28.52	42.08	31.68	25.34	49.60	25.19	31.73	26.59	21.27	45.16	27.53	31.45	25.52	20.41
UniSWM	**63.20**	**76.10**	**69.14**	**66.84**	**54.81**	**65.60**	**71.02**	**72.58**	**66.54**	**52.56**	**52.80**	**60.06**	**63.02**	**58.11**	**42.65**	**56.80**	**58.58**	**54.19**	**52.16**	**39.74**
Step																				
Qwen-VL-Max	41.60	17.66	33.58	19.65	15.72	39.20	14.92	26.71	17.06	13.65	49.60	19.77	31.18	21.07	16.85	45.60	20.09	30.09	18.09	14.47
GPT-5	54.47	34.65	48.13	34.79	27.83	49.60	33.85	42.21	30.78	24.62	54.47	28.36	39.91	26.30	21.04	52.80	33.93	46.64	32.20	25.76
Gemini-2.5-Pro	41.60	18.62	22.58	19.53	15.63	42.40	24.89	31.24	25.18	20.14	31.45	16.67	20.15	15.98	12.79	38.71	18.94	22.78	19.02	15.22
UniSWM	**49.60**	**23.64**	**31.50**	**24.25**	**19.02**	**52.00**	**23.00**	**42.97**	**28.35**	**20.92**	**64.80**	**30.51**	**39.30**	**30.08**	**25.25**	**55.20**	**30.09**	**41.56**	**31.37**	**25.39**

4.2 Evaluation of Long-Horizon Prediction

Phase prediction across horizons. As shown in Table 4, UniSWM leads by large margins at every horizon. At H=1s it attains $63.20/76.10/69.14/66.84/54.81$ (Acc./Pre./Rec./F1/Jac.), while the best baseline reaches only 21.00 Acc., 13.04 F1, and 7.42 Jac., yielding improvements of $+42.20$, $+53.80$, and $+47.39$ points. Performance remains strong as the look-ahead extends: $65.60/66.54/52.56$ at 5s, $52.80/58.11/42.65$ at 30s, and $56.80/52.16/39.74$ at 60s (Acc./F1/Jac.). Even at 60s, UniSWM exceeds the best baseline by large margins, indicating controlled error accumulation and reliable temporal credit assignment.

Step prediction and fine-grained stability. Step labels change more frequently and have higher cardinality, yet UniSWM maintains clear state tracking. Acc. rises from 49.60 at 1s to 52.00 at 5s, peaks at 64.80 at 30s, and remains 55.20 at 60s. F1 and Jac. improve with horizon ($24.25 \rightarrow 28.35 \rightarrow 30.08 \rightarrow 31.37$ and $19.02 \rightarrow 20.92 \rightarrow 25.25 \rightarrow 25.39$), suggesting that medium-range windows expose regularities that UniSWM exploits without sacrificing long-range stability. Recall gains are particularly large relative to baselines, while precision remains competitive.

Joint Phase&Step prediction. Joint decoding requires mutual consistency across the workflow hierarchy. UniSWM achieves $31.00/36.60/35.40/33.30$ Acc. at H=$1/5/30/60$s and delivers the highest F1 and Jac. at each horizon (e.g., 10.67 F1 and 7.57 Jac. at 5s), showing that action-aware latent dynamics encourage coherent transitions rather than optimizing each level in isolation.

Table 5: Results of Scene Initialization.

Model	In-body		Out-of-body	
	FID↓	Recall↑	FID↓	Recall↑
SD-3.5-Large	275.53	0.0020	118.01	0.1360
hunyuanimage-v2.1	308.46	0.0000	130.57	0.1520
FLUX.1-dev	324.01	0.0000	124.16	0.1580
Qwen-Image	260.83	0.0020	123.14	0.1580
Gemini2.5-Flash-Image	253.99	0.0000	172.27	0.0700
UniSWM	**59.58**	**0.7960**	**104.40**	**0.2520**

Table 6: Results of Scene Evolution.

Model	LPIPS↓	FID↓	KID↓	PSNR↑
FLUX.1-Kontext-dev	0.4734	81.56	0.0172 ± 0.0030	13.91 ± 2.19
Qwen-Image-Edit	0.2726	77.79	0.0193 ± 0.0041	17.90 ± 3.97
Gemini2.5-Flash-Image	0.3044	95.92	0.0145 ± 0.0000	16.61 ± 2.57
UniSWM	**0.2251**	**49.62**	**0.0033 ± 0.0019**	**18.51 ± 3.66**

Table 7: Fine-grained generation controlled by action and movement.

	Movement						**Action**					
Model	Type	LPIPS↓	FID↓	Recall↑	PSNR↑	SSIM↑	Type	LPIPS↓	FID↓	Recall↑	PSNR↑	SSIM↑
FLUX.1-Kontext-dev	Move Up	0.4768	117.70	0.2192	13.84	0.3010	Suture	0.4687	192.81	0.3043	14.17	0.2978
Qwen-Image-Edit		0.2858	116.28	0.4521	17.79	0.5632		0.2897	197.96	0.4348	17.11	0.5506
UniSWM		**0.2305**	**78.11**	**0.5982**	**18.43**	**0.5960**		**0.2029**	**132.67**	**0.7391**	**17.75**	**0.6590**
FLUX.1-Kontext-dev	Move Down	0.4881	159.74	0.2581	13.71	0.2977	Knotting	0.4757	237.84	0.7692	12.91	0.2518
Qwen-Image-Edit		0.2539	135.19	0.6022	18.12	0.5746		0.2694	236.68	0.6154	17.72	0.5653
UniSWM		**0.2277**	**97.66**	**0.6129**	**18.46**	**0.5813**		**0.1924**	**172.07**	**1.0000**	**19.24**	**0.6158**
FLUX.1-Kontext-dev	Move Left	0.4594	151.51	0.3553	14.19	0.3031	Dissection	0.4845	109.43	0.1882	13.93	0.3107
Qwen-Image-Edit		0.2910	157.97	0.5395	17.70	0.5416		0.2945	100.47	0.3727	17.52	0.5366
UniSWM		**0.2173**	**110.75**	**0.7500**	**18.83**	**0.5696**		**0.2504**	**70.04**	**0.4834**	**18.24**	**0.5441**
FLUX.1-Kontext-dev	Move Right	0.4524	157.15	0.4426	14.43	0.3125	Needle Puncture	0.4606	157.41	0.1500	13.56	0.2696
Qwen-Image-Edit		0.2681	163.51	0.5246	17.61	0.5620		0.1709	132.58	0.5833	20.01	0.7195
UniSWM		**0.2135**	**119.71**	**0.7213**	**18.59**	**0.5885**		**0.1345**	**79.59**	**0.6167**	**19.75**	**0.7324**
FLUX.1-Kontext-dev	Upper Left	0.4790	175.51	0.3333	14.03	0.3069	Tissue Retraction	0.4634	174.05	0.4524	14.20	0.2963
Qwen-Image-Edit		0.3153	174.47	0.4444	17.42	0.5350		0.2880	171.85	0.5000	17.78	0.5403
UniSWM		**0.2521**	**126.93**	**0.7143**	**18.25**	**0.5704**		**0.2436**	**126.12**	**0.6667**	**18.33**	**0.5535**
FLUX.1-Kontext-dev	Upper Right	0.4619	169.14	0.4211	14.01	0.2980	Needle Grasping	0.4460	161.32	0.3824	13.99	0.2914
Qwen-Image-Edit		0.2798	175.48	0.5263	18.11	0.5754		0.2490	173.57	0.5294	17.30	0.6019
UniSWM		**0.2339**	**120.20**	**0.7544**	**18.77**	**0.5997**		**0.1606**	**94.83**	**0.6471**	**18.75**	**0.7064**
FLUX.1-Kontext-dev	Lower Left	0.4803	164.53	0.3030	13.89	0.3062	Coagulation	0.4977	252.17	0.2500	14.40	0.3296
Qwen-Image-Edit		0.2728	159.37	0.5909	18.14	0.5592		0.2796	219.65	0.5000	18.60	0.5473
UniSWM		**0.2278**	**110.65**	**0.7273**	**18.47**	**0.5819**		**0.2216**	**182.22**	**0.7500**	**19.63**	**0.5586**
FLUX.1-Kontext-dev	Lower Right	0.4503	155.49	0.4462	14.39	0.3103	Aspiration	0.4437	178.64	0.4048	14.05	0.3104
Qwen-Image-Edit		0.2676	148.87	0.6000	18.21	0.5664		0.2586	178.64	0.5476	18.55	0.5487
UniSWM		**0.2343**	**114.89**	**0.7538**	**18.65**	**0.5706**		**0.2380**	**126.84**	**0.6905**	**18.69**	**0.5481**
FLUX.1-Kontext-dev	Move In	0.4882	159.71	0.2600	13.98	0.3062	Packing	0.5279	427.62	0.6667	11.66	0.2850
Qwen-Image-Edit		0.3009	160.86	0.4700	17.31	0.5460		0.4271	392.75	0.6667	13.13	0.4327
UniSWM		**0.2582**	**116.78**	**0.6600**	**17.97**	**0.5613**		**0.3729**	**394.83**	0.6667	**14.18**	**0.4662**
FLUX.1-Kontext-dev	Move Out	0.4764	145.75	0.2925	13.83	0.3111	**Overall**	0.4734	81.56	0.1580	13.91	0.3014
Qwen-Image-Edit		0.3266	152.49	0.4151	16.66	0.5066		0.2726	77.79	0.3460	17.90	0.5653
UniSWM		**0.2763**	**113.52**	**0.5094**	**17.61**	**0.5467**		**0.2251**	**49.62**	**0.3960**	**18.51**	**0.5859**

4.3 Evaluation of Fine-Grained Generation

Scene initialization. UniSWM achieves a substantial lead for both in-body and out-of-body synthesis. For in-body initialization, FID drops to 59.58 while Recall rises to 0.7960, compared to prior systems whose FID ranges from 253.99–324.01 and Recall is at or near zero (0.0000–0.0020). Out-of-body performance also improves: FID $= 104.40$ and Recall $= 0.2520$, outperforming strong baselines such as Qwen-Image (FID $= 123.14$, Recall $= 0.1580$) and FLUX.1-dev (FID $= 124.16$, Recall $= 0.1580$). These results indicate that UniSWM initializes anatomically plausible content with higher instance coverage, rather than relying on over-smoothed or generic surgical layouts.

Scene evolution. On in-body editing, UniSWM achieves the lowest LPIPS (0.2251), the best FID (49.62), the lowest KID (0.0033 ± 0.0019), and the highest PSNR (18.51 ± 3.66). Compared to Qwen-Image-Edit and FLUX.1-Kontext-dev, UniSWM improves fidelity and perceptual similarity simultaneously, suggesting that the learned latent dynamics allow edits that respect local tissue appearance and lighting while following requested controls.

Movement-conditioned control. UniSWM consistently secures the best tradeoff across LPIPS/FID/Recall/PSNR for directed camera/tool motions (e.g., *Move Up/Down/Left/Right*, diag-

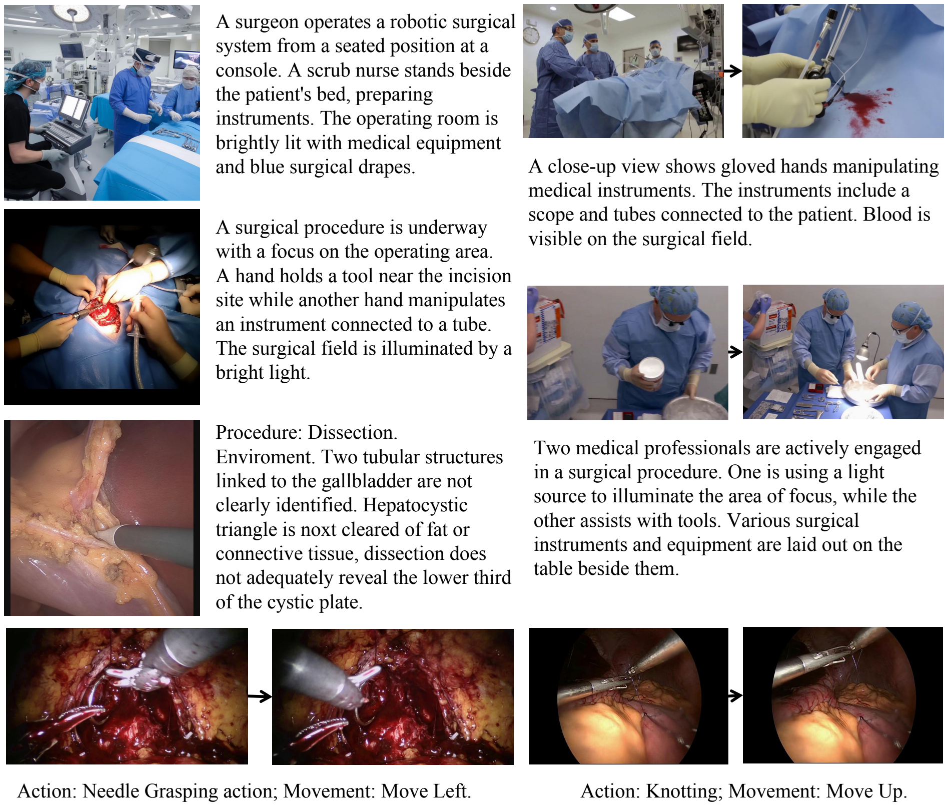

A surgeon operates a robotic surgical system from a seated position at a console. A scrub nurse stands beside the patient's bed, preparing instruments. The operating room is brightly lit with medical equipment and blue surgical drapes.

A surgical procedure is underway with a focus on the operating area. A hand holds a tool near the incision site while another hand manipulates an instrument connected to a tube. The surgical field is illuminated by a bright light.

Procedure: Dissection. Enviroment. Two tubular structures linked to the gallbladder are not clearly identified. Hepatocystic triangle is noxt cleared of fat or connective tissue, dissection does not adequately reveal the lower third of the cystic plate.

A close-up view shows gloved hands manipulating medical instruments. The instruments include a scope and tubes connected to the patient. Blood is visible on the surgical field.

Two medical professionals are actively engaged in a surgical procedure. One is using a light source to illuminate the area of focus, while the other assists with tools. Various surgical instruments and equipment are laid out on the table beside them.

Action: Needle Grasping action; Movement: Move Left.

Action: Knotting; Movement: Move Up.

Figure 2: Visualization of UniSWM

onals, and *Move In/Out*). Illustratively, for *Move Up* it reaches LPIPS = 0.2305, FID = 78.11, Recall = 0.5982, PSNR = 18.43, surpassing FLUX.1-Kontext-dev and Qwen-Image-Edit on all metrics. Similar margins are observed for *Move Right* (LPIPS = 0.2135, FID = 119.71, Recall = 0.7213, PSNR = 18.59) and *Lower Right* (LPIPS = 0.2343, FID = 114.89, Recall = 0.7538, PSNR = 18.65). These gains indicate that UniSWM's latent dynamics not only predict plausible motion fields but also synthesize the corresponding texture changes without drifting from the surgical context.

Action-conditioned control. For fine-grained manipulations (e.g., *Suture*, *Knotting*, *Dissection*, *Needle Puncture*, *Tissue Retraction*, *Needle Grasping*, *Coagulation*, *Aspiration*), UniSWM attains the best or tied-best results across metrics. For *Knotting* it attains perfect Recall = 1.0000 with LPIPS = 0.1924, FID = 172.07, PSNR = 19.24. The improvements persist on visually confusable categories such as *Dissection* (LPIPS = 0.2504, FID = 70.04, Recall = 0.4834, PSNR = 18.24) and *Needle Puncture* (LPIPS = 0.1345, FID = 79.59, Recall = 0.6167, PSNR = 19.75). These results suggest that UniSWM's action-aware latent transitions provide reliable control signals that map textual intent to surgical kinematics and contact states.

5 Conclusion

We propose UniSWM, a unified surgical world model that couples multimodal perception with hierarchy-aligned action and movement tokens and a Mixture-of-Transformers backbone to support three capabilities within a single architecture: structured understanding, long-horizon prediction, and fine-grained, controllable visual generation across both in-body and out-of-body settings. Alongside the model, we propose UniSWM-DB and UniSWM-Bench to stress-test recognition, forecasting, and movement/action-conditioned synthesis. Empirically, UniSWM sets advanced results on present-scene understanding, leads Phase and Step prediction at all horizons, and substantially improves both scene initialization and scene evolution while adhering to fine-grained controls.

Ethics statement

This work involves the use of surgical video data and multimodal annotations collected from multiple institutions. All data used in this study have been de-identified to remove any personally identifiable information. The dataset, UniSWM-DB, adheres to strict privacy and ethical standards, including compliance with HIPAA and GDPR regulations, and has been anonymized to prevent re-identification of patients or personnel.

We also recognize the importance of fairness and bias mitigation. While our dataset is diverse across institutions and surgical procedures, we encourage further efforts to ensure equitable representation across demographics and surgical contexts. No harmful applications or discriminatory behaviors are intended or supported by this work.

Reprodicibility statement

To support reproducibility, we provide the following resources and methodological details:

- The UniSWM-DB dataset is described in Section 4, including annotation schemas, preprocessing steps, and data splits for temporal, cross-site, and cross-view evaluation. A data card summarizes ethical compliance, licensing, and usage guidelines is also included.
- The full architectural details of UniSWM, including the Mixture-of-Transformers design, latent dynamics modeling, and decoder specifications, are given in Section 3.
- UniSWM-Bench is introduced with task definitions, evaluation protocols, and metrics for understanding, prediction, and generation tasks. All benchmark splits and evaluation scripts are documented.

REFERENCES

Max Allan, Alex Shvets, Thomas Kurmann, Zichen Zhang, Rahul Duggal, Yun-Hsuan Su, Nicola Rieke, Iro Laina, Niveditha Kalavakonda, Sebastian Bodenstedt, et al. 2017 robotic instrument segmentation challenge. *arXiv preprint arXiv:1902.06426*, 2019.

Anthony Brohan, Noah Brown, Justice Carbajal, et al. RT-2: Vision-language-action models transfer web knowledge to robotic control. *arXiv preprint arXiv:2307.15818*, 2023.

CAMMA Lab. Cholec80 dataset. `https://camma.unistra.fr/datasets/`. Accessed 2025-09-21.

Hanqun Cao, Cheng Tan, Zhangyang Gao, Yilun Xu, Guangyong Chen, Pheng-Ann Heng, and Stan Z Li. A survey on generative diffusion models. *IEEE transactions on knowledge and data engineering*, 36(7):2814–2830, 2024.

Joseph Cho, Samuel Schmidgall, Cyril Zakka, Mrudang Mathur, Dhamanpreet Kaur, Rohan Shad, and William Hiesinger. SurGen: Text-guided diffusion model for surgical video generation. *arXiv preprint arXiv:2408.14028*, 2024.

Kubilay Can Demir, Hannah Schieber, Tobias Weise, Daniel Roth, Matthias May, Andreas Maier, and Seung Hee Yang. Deep learning in surgical workflow analysis: a review of phase and step recognition. *IEEE Journal of Biomedical and Health Informatics*, 27(11):5405–5417, 2023.

Hao Ding, Lalithkumar Seenivasan, Benjamin D Killeen, Sue Min Cho, and Mathias Unberath. Digital twins as a unifying framework for surgical data science: the enabling role of geometric scene understanding. *Artificial Intelligence Surgery*, 4(3), 2024a.

Jingtao Ding, Yunke Zhang, Yu Shang, Yuheng Zhang, Zefang Zong, Jie Feng, Yuan Yuan, Hongyuan Su, Nian Li, Nicholas Sukiennik, et al. Understanding world or predicting future? a comprehensive survey of world models. *ACM Computing Surveys*, 2024b.

Danny Driess, Fei Xia, Pierre Sermanet, et al. PaLM-E: An embodied multimodal language model. In *Proceedings of the International Conference on Learning Representations (ICLR)*. PMLR, 2023.

Fernando Pérez Escamirosa, Ricardo Manuel Ordorica Flores, Ignacio Oropesa García, Cristian Rubén Zalles Vidal, and Arturo Minor Martínez. Face, content, and construct validity of the endovis training system for objective assessment of psychomotor skills of laparoscopic surgeons. *Surgical endoscopy*, 29(11):3392–3403, 2015.

David Ha and Jürgen Schmidhuber. World models. *arXiv preprint arXiv:1803.10122*, 2018.

Danijar Hafner, Timothy Lillicrap, Jimmy Ba, and Mohammad Norouzi. Dream to control: Learning behaviors by latent imagination. *arXiv preprint arXiv:1912.01603*, 2019.

Idris Hamoud, Vinkle Srivastav, Muhammad Abdullah Jamal, Didier Mutter, Omid Mohareri, and Nicolas Padoy. Multi-view video-pose pretraining for operating room surgical activity recognition. *arXiv preprint arXiv:2502.13883*, 2025.

Shibo Hao, Yi Gu, Haodi Ma, Joshua Jiahua Hong, Zhen Wang, Daisy Zhe Wang, and Zhiting Hu. Reasoning with language model is planning with world model. *arXiv preprint arXiv:2305.14992*, 2023.

Jonathan Ho, Ajay Jain, and Pieter Abbeel. Denoising diffusion probabilistic models. In *Advances in Neural Information Processing Systems (NeurIPS)*, 2020.

Ivan Iliash, Manuel Wiesenfarth, Nicola Rieke, and Stefanie Speidel. Interactive generation of laparoscopic videos with diffusion models. *arXiv preprint arXiv:2406.06537*, 2024.

Yueming Jin, Yonghao Long, Cheng Chen, Zixu Zhao, Qi Dou, and Pheng-Ann Heng. Temporal memory relation network for workflow recognition from surgical video. *arXiv preprint arXiv:2103.16327*, 2021.

Ufaq Khan, Umair Nawaz, Adnan Qayyum, Shazad Ashraf, Muhammad Bilal, and Junaid Qadir. Surgical scene understanding in the era of foundation ai models: A comprehensive review. *arXiv preprint arXiv:2502.14886*, 2025.

Minjong Kim, Chenfeng Meng, Di Zhang, et al. OpenVLA: An open-source vision-language-action model. In *Proceedings of the International Conference on Machine Learning (ICML)*, volume 270 of *Proceedings of Machine Learning Research*. PMLR, 2025.

Chenhao Li, Andreas Krause, and Marco Hutter. Robotic world model: A neural network simulator for robust policy optimization in robotics. *arXiv preprint arXiv:2501.10100*, 2025.

Guanxing Lu, Wenkai Guo, Chubin Zhang, Yuheng Zhou, Haonan Jiang, Zifeng Gao, Yansong Tang, and Ziwei Wang. Vla-rl: Towards masterful and general robotic manipulation with scalable reinforcement learning. *arXiv preprint arXiv:2505.18719*, 2025.

Yueen Ma, Zixing Song, Yuzheng Zhuang, Jianye Hao, and Irwin King. A survey on vision-language-action models for embodied ai. *arXiv preprint arXiv:2405.14093*, 2024.

Zhe Min, Jiewen Lai, and Hongliang Ren. Innovating robot-assisted surgery through large vision models. *Nature Reviews Electrical Engineering*, pp. 1–14, 2025.

Angie M Paik, Leila J Mady, Aditya Sood, and Edward S Lee. Beyond the operating room: a look at legal liability in body contouring procedures. *Aesthetic surgery journal*, 34(1):106–113, 2014.

Robin Rombach, Andreas Blattmann, Dominik Lorenz, Patrick Esser, and Björn Ommer. High-resolution image synthesis with latent diffusion models. In *Proceedings of the IEEE/CVF Conference on Computer Vision and Pattern Recognition (CVPR)*, pp. 10684–10695, 2022.

Adam Schmidt, Aidean Sharghi, Helene Haugerud, Daniel Oh, and Omid Mohareri. Multi-view surgical video action detection via mixed global view attention. In *International conference on medical image computing and computer-assisted intervention*, pp. 626–635. Springer, 2021.

Vinkle Srivastav, Thibaut Issenhuth, Abdolrahim Kadkhodamohammadi, Michel de Mathelin, Afshin Gangi, and Nicolas Padoy. MVOR: A multi-view RGB-D operating room dataset for 2d and 3d human pose estimation. *arXiv preprint arXiv:1808.08180*, 2018.

Andru P Twinanda, Sherif Shehata, Didier Mutter, Jacques Marescaux, Michel de Mathelin, and Nicolas Padoy. EndoNet: A deep architecture for recognition tasks on laparoscopic videos. *IEEE Transactions on Medical Imaging*, 36(1):86–97, 2017. doi: 10.1109/TMI.2016.2593957.

Jiannan Xiang, Tianhua Tao, Yi Gu, Tianmin Shu, Zirui Wang, Zichao Yang, and Zhiting Hu. Language models meet world models: Embodied experiences enhance language models. *Advances in neural information processing systems*, 36:75392–75412, 2023.

Zhitao Zeng, Guojian Yuan, Junyuan Mao, Yuxuan Wang, Xiaoshuang Jia, and Yueming Jin. Multi-scale temporal prediction via incremental generation and multi-agent collaboration, 2025a. URL `https://arxiv.org/abs/2509.17429`.

Zhitao Zeng, Zhu Zhuo, Xiaojun Jia, Erli Zhang, Junde Wu, Jiaan Zhang, Yuxuan Wang, Chang Han Low, Jian Jiang, Zilong Zheng, et al. Surgvlm: A large vision-language model and systematic evaluation benchmark for surgical intelligence. *arXiv preprint arXiv:2506.02555*, 2025b.

Changyuan Zhao, Guangyuan Liu, Ruichen Zhang, Yinqiu Liu, Jiacheng Wang, Jiawen Kang, Dusit Niyato, Zan Li, Zhu Han, Sumei Sun, et al. Edge general intelligence through world models and agentic ai: Fundamentals, solutions, and challenges. *arXiv preprint arXiv:2508.09561*, 2025a.

Qingqing Zhao, Yao Lu, Moo Jin Kim, Zipeng Fu, Zhuoyang Zhang, Yecheng Wu, Zhaoshuo Li, Qianli Ma, Song Han, Chelsea Finn, et al. Cot-vla: Visual chain-of-thought reasoning for vision-language-action models. In *Proceedings of the Computer Vision and Pattern Recognition Conference*, pp. 1702–1713, 2025b.

A Related Work (Extended)

A.1 World Models and Latent Dynamics

Early world models demonstrated that compact latent rollouts enable planning directly from pixels (Ha & Schmidhuber, 2018). Dreamer-style algorithms introduced stochastic latent imagination with actor–critic learning to improve stability and sample efficiency for continuous control (Hafner et al., 2019). Recent works explore scaling latent sequence modeling and credit assignment for longer horizons and complex tasks (Hao et al., 2023). In parallel, diffusion modeling—from denoising diffusion to latent diffusion—has delivered state-of-the-art image and video synthesis fidelity, offering stronger priors for forward prediction, temporal consistency, and controllability (Ho et al., 2020; Rombach et al., 2022; Cao et al., 2024). UniSWM leverages these trajectories by coupling latent dynamics for prediction with high-fidelity generative pathways for controllable synthesis.

A.2 Multimodal Foundation Models and VLA Policies

The emergence of vision–language(-action) models has connected internet-scale knowledge with embodied decision making (Ma et al., 2024). Systems such as RT-2 utilize vision–language pretraining to ground robotic policies in open-world concepts (Brohan et al., 2023), while foundation models like PaLM-E unify perception and language for downstream control (Driess et al., 2023). OpenVLA-style frameworks further emphasize generalization via modular perception–policy stacks (Kim et al., 2025). These trends suggest a path to unify recognition, prediction, and controllable synthesis, where a single backbone can interpret scenes, anticipate future states, and generate task-aligned visuals. UniSWM follows this direction but is specialized for surgical constraints, emphasizing safety, cross-view robustness, and action-/movement-aware control.

A.3 Surgical Intelligence: Perception, Workflow, and Context

Surgical scene understanding covers phase/step recognition, instrument detection and segmentation, and workflow modeling (Demir et al., 2023; Ding et al., 2024a). Foundational works on endoscopic phase recognition (e.g., Cholec80) established supervised temporal modeling for intraoperative guidance (Twinanda et al., 2017; CAMMA Lab), followed by architectures that leverage spatiotemporal cues and attention (Jin et al., 2021). Community benchmarks broadened evaluation beyond in-body views: EndoVis instrument segmentation and MVOR OR datasets examine tool presence, segmentation quality, and staff/activity context under multi-view settings (Escamirosa et al., 2015; Allan et al., 2019; Srivastav et al., 2018). Despite progress, unified modeling that (i) spans in-body and out-of-body signals, (ii) performs long-horizon prediction of workflow states, and (iii) supports controllable visual synthesis remains limited.

A.4 Surgical Video Synthesis and Controllable Editing

Recent diffusion-based efforts explore surgical video generation and interactive editing (Cho et al., 2024; Iliash et al., 2024). Controllable surgical synthesis is particularly challenging: models must adhere to instrument kinematics, preserve tissue realism, and respect safety constraints while following fine-grained action or movement commands. Emerging work on multi-scale temporal prediction and incremental evolution seeks to stabilize long-horizon edits by aligning local texture updates with global intent (Zeng et al., 2025a). However, most systems still treat perception, prediction, and generation as separate modules, which can lead to temporal drift, inconsistent tool–tissue interactions, or suboptimal adherence to requested controls.

A.5 Positioning of UniSWM

UniSWM differs from prior art in three ways. *First*, it unifies structured understanding (phase, action, relations, grounding), long-horizon prediction (phase, step, and joint targets), and controllable generation (movement- and action-conditioned) within one framework, reducing cross-module mismatch. *Second*, it operates across in-body and out-of-body settings, enabling cross-view consistency and broader clinical coverage. *Third*, its generation pathway is designed to respect surgical plausibility (instrument kinematics, tissue appearance) while following fine-grained controls, addressing common failure modes observed in prior diffusion-based pipelines (Cho et al., 2024; Iliash et al., 2024). Together with lessons from world models and VLA systems (Ha & Schmidhuber, 2018; Hafner et al., 2019; Ma et al., 2024; Brohan et al., 2023; Driess et al., 2023; Kim et al., 2025; Ho et al., 2020; Rombach et al., 2022), UniSWM targets a practical middle ground between predictive modeling and controllable synthesis tailored to surgical domains.

Scope and Limitations. While UniSWM advances unified modeling for surgical AI, the broader literature continues to expand in data scale, multimodal sensing (e.g., depth, audio, kinematics), and evaluation protocols. Our focus on phase/step dynamics and tool–tissue interactions complements, rather than replaces, specialized lines in registration, reconstruction, and simulation. We view UniSWM as a step toward integrated systems that couple reliable understanding and prediction with safe, user-controllable generation in real surgical workflows.

B Experiments

Table 8: Stability analysis of phase recognition (Max/Min/Mean across temperatures 0.5, 0.6, 0.7). Values are shown as percentages.

Model	Accuracy Mean (Min, Max)	Recall Mean (Min, Max)	Precision Mean (Min, Max)	Jaccard Mean (Min, Max)
SmolVLM2-2.2B	20.81 (20.13, 21.80)	15.37 (13.95, 16.90)	12.18 (11.08, 13.84)	6.35 (5.90, 7.19)
Skywork-R1V-38B	6.94 (6.81, 7.11)	14.31 (14.24, 14.41)	17.24 (11.27, 28.55)	1.56 (1.31, 1.88)
Phi4-Multimodal	17.92 (13.95, 20.82)	15.50 (13.47, 17.40)	14.14 (10.57, 19.25)	5.36 (3.89, 6.70)
Mistral-Small-24B	25.60 (23.45, 28.25)	25.92 (23.88, 27.42)	26.80 (23.78, 30.69)	11.64 (10.56, 12.73)
PaliGemma2-3B	7.29 (6.50, 7.75)	13.90 (12.38, 15.42)	10.08 (6.73, 12.10)	2.35 (2.02, 2.75)
Llama-4-Scout-17B-16E	40.70 (40.40, 41.30)	18.02 (17.59, 18.44)	27.96 (27.22, 29.14)	8.71 (8.53, 8.94)
Kimi-VL-A3B-Instruct	35.00 (33.60, 36.30)	19.04 (18.27, 20.04)	20.79 (18.35, 22.56)	10.25 (9.57, 10.77)
Kimi-VL-A3B-Thinking	6.53 (6.40, 6.60)	14.31 (14.15, 14.43)	16.61 (7.00, 21.52)	1.06 (0.97, 1.16)
Gemma3-27B	14.03 (14.00, 14.10)	16.93 (16.52, 17.25)	25.37 (15.64, 30.72)	4.52 (4.23, 4.81)
MiMo-VL-7B-SFT	20.90 (20.30, 22.10)	16.46 (14.81, 17.91)	20.73 (15.93, 29.04)	7.15 (6.85, 7.40)
MiMo-VL-7B-RL	25.73 (23.40, 27.90)	14.77 (13.82, 15.44)	15.73 (15.31, 16.45)	6.77 (6.50, 6.98)
MiniCPM-V-2_6	16.85 (15.29, 18.56)	14.20 (11.87, 17.09)	14.24 (12.64, 16.09)	6.10 (5.30, 7.30)
MiniCPM-o-2_6	15.10 (13.41, 16.40)	20.63 (20.21, 21.08)	23.77 (22.17, 24.70)	8.68 (8.27, 8.94)
Qwen-Omni-3B	34.16 (32.50, 36.20)	18.27 (17.64, 18.87)	18.11 (17.02, 19.73)	10.59 (10.25, 10.78)
Qwen-Omni-7B	22.01 (21.42, 22.50)	18.10 (15.57, 19.39)	18.16 (14.53, 23.07)	7.66 (6.87, 8.26)
Qwen2.5-VL-7B	27.57 (27.40, 27.90)	18.48 (17.73, 19.46)	20.50 (19.29, 22.06)	8.33 (8.10, 8.60)
Qwen2.5-VL-32B	44.77 (44.70, 44.90)	22.05 (21.89, 22.18)	26.83 (23.95, 29.77)	13.63 (13.46, 13.83)
Qwen2.5-VL-72B	37.03 (35.70, 37.80)	20.21 (19.83, 20.85)	23.75 (21.34, 26.03)	10.82 (9.98, 11.48)
InternVL3-8B	30.93 (30.00, 32.10)	19.38 (18.40, 20.63)	22.21 (17.02, 25.19)	10.71 (9.42, 11.82)
InternVL3-78B	33.17 (31.70, 34.50)	25.25 (23.30, 26.74)	34.01 (29.06, 42.27)	15.05 (13.88, 15.88)
MedVLM-R1	10.50 (10.40, 10.70)	16.15 (15.97, 16.45)	12.54 (11.90, 13.74)	2.40 (2.28, 2.50)
Lingshu-7B	39.77 (39.60, 39.90)	23.53 (23.22, 23.88)	13.63 (12.36, 14.67)	9.07 (8.84, 9.32)
Lingshu-32B	36.31 (34.20, 38.70)	22.22 (20.96, 24.44)	23.98 (19.95, 29.19)	12.85 (11.45, 15.10)
MedGemma-4B	27.07 (25.90, 27.70)	23.33 (22.76, 24.09)	18.53 (17.29, 19.48)	9.63 (9.11, 9.91)
MedGemma-27B	43.40 (43.00, 43.60)	15.30 (15.12, 15.66)	24.68 (23.88, 25.75)	7.37 (7.14, 7.71)
SurgVLM-72B	73.05 (72.83, 73.29)	65.30 (64.98, 65.63)	64.91 (64.60, 65.36)	49.10 (48.73, 49.56)
UniSWM	**79.73 (76.70, 81.90)**	**67.11 (65.07, 68.66)**	**70.54 (69.76, 71.79)**	**52.88 (50.63, 54.42)**

Table 9: Stability analysis of action recognition (Max/Min/Mean across temperatures 0.5, 0.6, 0.7). Values are shown as percentages.

Model	Accuracy Mean (Min, Max)	Recall Mean (Min, Max)	Precision Mean (Min, Max)	Jaccard Mean (Min, Max)
SmolVLM2-2.2B	14.93 (14.70, 15.30)	12.25 (11.69, 12.99)	13.05 (12.20, 14.09)	5.61 (5.50, 5.78)
Skywork-R1V-38B	11.83 (11.70, 12.00)	12.62 (12.42, 13.02)	14.42 (13.35, 15.30)	2.76 (2.68, 2.84)
Phi4-Multimodal	24.37 (23.10, 25.10)	12.38 (11.71, 12.88)	13.35 (9.20, 20.92)	5.74 (5.35, 6.02)
Mistral-Small-24B	12.50 (12.40, 12.60)	12.68 (12.57, 12.74)	5.73 (5.47, 6.06)	1.78 (1.76, 1.82)
PaliGemma2-3B	11.57 (11.00, 12.40)	12.58 (12.00, 13.11)	13.92 (10.33, 17.60)	2.26 (2.15, 2.46)
Llama-4-Scout-17B-16E	30.97 (30.50, 31.20)	12.75 (12.53, 12.90)	19.46 (18.90, 19.99)	4.66 (4.52, 4.79)
Kimi-VL-A3B-Instruct	25.23 (24.30, 25.70)	14.17 (12.20, 15.31)	12.10 (10.05, 13.97)	6.91 (5.84, 7.67)
Kimi-VL-A3B-Thinking	11.23 (10.70, 11.70)	12.90 (12.14, 13.61)	14.07 (5.93, 23.81)	2.33 (2.11, 2.46)
Gemma3-27B	31.97 (31.90, 32.00)	13.50 (13.47, 13.52)	20.60 (16.43, 22.69)	5.01 (4.97, 5.03)
MiMo-VL-7B-SFT	24.37 (23.60, 25.00)	15.72 (14.68, 17.26)	17.56 (11.09, 25.74)	7.40 (6.49, 8.56)
MiMo-VL-7B-RL	26.90 (24.60, 28.30)	14.04 (12.87, 14.81)	14.21 (11.23, 18.64)	7.05 (6.39, 7.68)
MiniCPM-V-2_6	24.43 (22.00, 26.60)	13.42 (11.41, 15.29)	14.14 (12.35, 16.84)	7.41 (6.44, 8.41)
MiniCPM-o-2_6	29.67 (28.90, 30.20)	12.47 (12.10, 12.71)	12.60 (10.08, 14.82)	5.22 (4.96, 5.59)
Qwen-Omni-3B	28.23 (27.40, 29.10)	12.38 (12.15, 12.80)	12.76 (12.13, 13.08)	5.69 (5.14, 6.12)
Qwen-Omni-7B	29.93 (29.60, 30.50)	13.20 (12.93, 13.34)	29.58 (23.54, 39.81)	5.81 (5.60, 6.22)
Qwen2.5-VL-7B	31.17 (31.10, 31.30)	12.55 (12.50, 12.66)	5.82 (3.89, 9.68)	4.02 (3.89, 4.29)
Qwen2.5-VL-32B	31.67 (31.50, 31.80)	13.72 (13.43, 14.18)	31.84 (29.80, 35.03)	5.34 (4.92, 5.99)
Qwen2.5-VL-72B	28.83 (27.30, 30.30)	13.42 (12.72, 14.03)	16.52 (15.93, 17.23)	6.21 (5.85, 6.54)
InternVL3-8B	29.30 (27.80, 30.60)	13.03 (12.38, 13.84)	14.16 (9.65, 22.85)	6.36 (6.12, 6.81)
InternVL3-78B	28.77 (28.10, 29.70)	12.69 (12.51, 12.98)	21.24 (18.27, 22.93)	6.22 (5.94, 6.39)
MedVLM-R1	31.13 (31.10, 31.20)	12.52 (12.51, 12.55)	16.39 (16.39, 16.40)	3.94 (3.94, 3.95)
Lingshu-7B	31.50 (31.40, 31.60)	12.92 (12.82, 13.03)	16.41 (16.41, 16.41)	4.33 (4.23, 4.44)
Lingshu-32B	26.60 (25.20, 27.50)	17.96 (16.45, 19.10)	20.07 (17.17, 21.64)	10.09 (9.34, 10.66)
MedGemma-4B	22.50 (22.30, 22.90)	12.32 (12.08, 12.48)	4.42 (3.74, 4.84)	3.53 (3.41, 3.61)
MedGemma-27B	29.90 (29.50, 30.30)	12.38 (12.18, 12.58)	20.73 (17.78, 24.71)	4.73 (4.55, 4.88)
SurgVLM-72B	45.13 (44.95, 45.35)	31.88 (31.28, 32.46)	30.05 (29.64, 30.79)	18.60 (18.36, 18.91)
UniSWM	**58.53 (53.20, 63.40)**	**40.08 (35.44, 42.77)**	**49.82 (42.19, 57.44)**	**28.25 (23.57, 31.34)**

Table 10: Stability analysis of triplet recognition (Max/Min/Mean across temperatures 0.5, 0.6, 0.7). Values are shown as percentages.

Model	Accuracy Mean (Min, Max)	Accuracy$_{ins}$ Mean (Min, Max)	Accuracy$_{ver}$ Mean (Min, Max)	Accuracy$_{tar}$ Mean (Min, Max)
SmolVLM2-2.2B	0.00 (0.00, 0.00)	7.87 (7.50, 8.48)	3.71 (3.23, 4.44)	0.62 (0.35, 1.15)
Skywork-R1V-38B	0.12 (0.12, 0.12)	21.06 (20.31, 22.50)	9.33 (9.12, 9.58)	2.25 (1.73, 2.71)
Phi4-Multimodal	0.29 (0.12, 0.46)	11.50 (9.52, 13.10)	12.58 (12.00, 12.98)	3.87 (3.46, 4.10)
Mistral-Small-24B	0.50 (0.29, 0.69)	9.08 (8.42, 9.46)	8.79 (8.60, 9.12)	5.96 (5.48, 6.46)
PaliGemma2-3B	0.00 (0.00, 0.00)	0.96 (0.23, 1.56)	2.19 (1.67, 3.17)	3.06 (2.54, 3.98)
Llama-4-Scout-17B-16E	0.21 (0.12, 0.29)	3.35 (2.94, 3.58)	3.56 (3.35, 3.75)	7.46 (6.52, 8.02)
Kimi-VL-A3B-Instruct	0.02 (0.00, 0.06)	12.04 (9.92, 14.60)	9.83 (9.29, 10.21)	2.14 (2.02, 2.19)
Kimi-VL-A3B-Thinking	0.04 (0.00, 0.12)	6.50 (5.94, 6.98)	9.21 (9.00, 9.52)	1.08 (0.75, 1.27)
Gemma3-27B	0.13 (0.12, 0.17)	10.00 (9.81, 10.33)	6.35 (5.94, 6.69)	1.67 (1.38, 1.85)
MiMo-VL-7B-SFT	0.13 (0.12, 0.17)	7.98 (7.16, 8.89)	5.10 (4.73, 5.42)	4.85 (4.33, 5.37)
MiMo-VL-7B-RL	0.21 (0.12, 0.29)	6.25 (5.77, 6.75)	5.14 (4.67, 5.65)	2.14 (1.85, 2.31)
MiniCPM-V-2_6	0.04 (0.00, 0.12)	17.02 (14.95, 18.29)	13.93 (13.16, 14.66)	1.35 (1.27, 1.38)
MiniCPM-o-2_6	0.35 (0.12, 0.46)	23.31 (22.74, 24.06)	8.92 (8.37, 9.87)	5.29 (4.90, 5.83)
Qwen-Omni-3B	0.00 (0.00, 0.00)	10.33 (9.69, 11.02)	7.06 (6.87, 7.21)	1.31 (1.04, 1.50)
Qwen-Omni-7B	0.15 (0.12, 0.23)	10.79 (10.39, 11.14)	6.87 (6.17, 7.33)	5.46 (4.85, 6.06)
Qwen2.5-VL-7B	0.23 (0.12, 0.29)	9.92 (9.12, 10.39)	4.65 (4.21, 4.90)	5.21 (4.56, 6.12)
Qwen2.5-VL-32B	0.23 (0.17, 0.29)	26.22 (25.79, 26.49)	6.69 (6.58, 6.75)	2.10 (1.73, 2.42)
Qwen2.5-VL-72B	0.19 (0.17, 0.23)	26.33 (25.97, 26.60)	8.16 (7.91, 8.31)	4.58 (4.39, 4.90)
InternVL3-8B	1.65 (1.56, 1.73)	51.49 (50.72, 52.39)	8.87 (8.71, 8.94)	24.39 (23.72, 24.99)
InternVL3-78B	0.37 (0.23, 0.52)	37.39 (34.85, 39.35)	8.54 (7.73, 9.41)	3.44 (2.31, 4.50)
MedVLM-R1	0.02 (0.00, 0.06)	45.72 (45.30, 46.28)	8.98 (8.94, 9.06)	0.31 (0.23, 0.40)
Lingshu-7B	0.08 (0.00, 0.12)	2.15 (1.85, 2.48)	7.98 (7.73, 8.37)	3.65 (3.29, 4.10)
Lingshu-32B	0.21 (0.12, 0.29)	21.04 (20.83, 21.29)	7.17 (6.29, 8.14)	3.77 (3.58, 3.87)
MedGemma-4B	0.00 (0.00, 0.00)	2.89 (2.65, 3.29)	8.17 (7.67, 8.54)	1.42 (1.15, 1.67)
MedGemma-27B	0.13 (0.12, 0.17)	8.39 (7.56, 9.29)	3.65 (3.46, 3.87)	3.62 (3.35, 4.10)
SurgVLM-72B	4.91 (4.88, 4.96)	47.66 (47.46, 47.78)	12.91 (12.81, 13.01)	38.91 (38.14, 39.41)
UniSWM	**49.73 (45.15, 55.11)**	**81.97 (80.08, 83.31)**	**70.88 (66.69, 74.90)**	**54.22 (50.67, 57.74)**

Table 11: Stability analysis of instrument grounding (Max/Min/Mean across temperatures 0.5, 0.6, 0.7). Values are shown as percentages.

Model	mIoU Mean (Min, Max)	mAP@0.5 Mean (Min, Max)	mAP@0.75 Mean (Min, Max)	COCO AP Mean (Min, Max)
SmolVLM2-2.2B	2.89 (2.72, 3.01)	0.27 (0.20, 0.30)	0.07 (0.00, 0.10)	0.08 (0.07, 0.09)
Skywork-R1V-38B	9.86 (9.46, 10.10)	1.60 (1.30, 2.00)	0.00 (0.00, 0.00)	0.28 (0.25, 0.32)
Phi4-Multimodal	1.17 (1.05, 1.36)	0.13 (0.00, 0.40)	0.00 (0.00, 0.00)	0.04 (0.00, 0.11)
Mistral-Small-24B	17.64 (17.08, 18.43)	5.93 (5.40, 6.30)	0.27 (0.10, 0.40)	1.45 (1.25, 1.60)
PaliGemma2-3B	0.01 (0.00, 0.03)	0.00 (0.00, 0.00)	0.00 (0.00, 0.00)	0.00 (0.00, 0.00)
Llama-4-Scout-17B-16E	36.72 (36.45, 37.27)	35.73 (35.50, 36.20)	7.17 (6.50, 7.80)	12.99 (12.92, 13.08)
Kimi-VL-A3B-Instruct	9.63 (8.58, 10.94)	4.93 (3.90, 6.10)	0.73 (0.30, 1.30)	1.62 (1.28, 2.23)
Kimi-VL-A3B-Thinking	9.36 (9.03, 9.91)	1.90 (1.80, 2.00)	0.13 (0.00, 0.30)	0.48 (0.39, 0.55)
Gemma3-27B	17.45 (17.06, 17.72)	6.17 (6.00, 6.30)	0.10 (0.10, 0.10)	1.41 (1.34, 1.51)
MiMo-VL-7B-SFT	33.45 (32.09, 34.70)	28.57 (26.30, 30.50)	2.80 (2.30, 3.80)	8.55 (7.78, 9.30)
MiMo-VL-7B-RL	36.86 (36.55, 37.31)	34.77 (33.90, 35.30)	3.77 (3.70, 3.90)	10.78 (10.51, 11.09)
MiniCPM-V-2_6	17.87 (16.13, 19.30)	7.33 (5.90, 8.20)	0.57 (0.40, 0.80)	1.87 (1.47, 2.14)
MiniCPM-o-2_6	20.33 (18.70, 22.43)	9.80 (8.20, 12.30)	1.10 (0.80, 1.40)	2.96 (2.45, 3.85)
Qwen-Omni-3B	22.17 (20.52, 23.61)	16.20 (14.10, 18.00)	3.47 (2.30, 4.70)	6.25 (5.06, 7.44)
Qwen-Omni-7B	34.60 (33.53, 35.68)	40.53 (38.30, 42.10)	5.63 (4.70, 6.60)	14.17 (13.35, 15.23)
Qwen2.5-VL-7B	10.63 (10.44, 10.84)	0.97 (0.60, 1.30)	0.03 (0.00, 0.10)	0.26 (0.20, 0.32)
Qwen2.5-VL-32B	11.36 (11.13, 11.55)	1.93 (1.60, 2.30)	1.07 (0.90, 1.30)	1.03 (0.87, 1.24)
Qwen2.5-VL-72B	42.70 (42.67, 42.72)	45.95 (45.60, 46.30)	25.75 (25.20, 26.30)	25.69 (25.25, 26.13)
InternVL3-8B	22.49 (22.14, 22.81)	7.13 (6.70, 7.80)	0.20 (0.10, 0.30)	1.58 (1.45, 1.78)
InternVL3-78B	29.41 (28.38, 30.39)	18.20 (17.40, 18.80)	1.60 (1.20, 2.00)	4.99 (4.60, 5.20)
MedVLM-R1	5.31 (5.29, 5.33)	0.30 (0.30, 0.30)	0.00 (0.00, 0.00)	0.03 (0.03, 0.03)
Lingshu-7B	28.72 (28.67, 28.80)	26.13 (25.80, 26.50)	3.37 (2.70, 3.80)	8.20 (7.92, 8.37)
Lingshu-32B	26.03 (24.72, 27.01)	18.20 (16.90, 19.70)	2.90 (2.40, 3.70)	5.89 (5.40, 6.58)
MedGemma-4B	9.43 (9.20, 9.70)	0.57 (0.20, 0.80)	0.00 (0.00, 0.00)	0.08 (0.02, 0.12)
MedGemma-27B	17.20 (17.08, 17.36)	2.23 (2.10, 2.40)	0.00 (0.00, 0.00)	0.44 (0.39, 0.48)
SurgVLM-72B	59.34 (59.14, 59.50)	74.20 (73.30, 74.80)	28.30 (27.90, 28.90)	36.28 (36.13, 36.46)
UniSWM	**86.41 (84.63, 88.11)**	**92.90 (92.00, 94.20)**	**87.43 (85.70, 88.70)**	**69.76 (65.97, 73.75)**

Table 12: Stability analysis of environment answering (Max/Min/Mean across temperatures 0.5, 0.6, 0.7). Values are shown as percentages.

Model	Accuracy Mean (Min, Max)	BLEU-4 Mean (Min, Max)	METEOR Mean (Min, Max)	ROUGE-1 Mean (Min, Max)
SmolVLM2-2.2B	23.65 (22.22, 25.64)	3.03 (1.80, 4.73)	12.19 (5.26, 21.15)	15.60 (7.92, 25.06)
Skywork-R1V-38B	35.63 (34.90, 36.41)	0.32 (0.26, 0.37)	1.36 (1.23, 1.54)	1.56 (1.35, 1.73)
Phi4-Multimodal	34.25 (34.03, 34.55)	0.34 (0.33, 0.36)	1.48 (1.41, 1.58)	1.74 (1.67, 1.84)
Mistral-Small-24B	36.79 (36.13, 37.34)	0.15 (0.11, 0.17)	0.59 (0.52, 0.64)	0.71 (0.58, 0.78)
PaliGemma2-3B	31.78 (31.61, 31.99)	1.55 (1.36, 1.71)	5.65 (4.78, 6.18)	9.04 (7.94, 9.78)
Llama-4-Scout-17B-16E	36.99 (36.54, 37.23)	0.04 (0.03, 0.04)	0.20 (0.18, 0.22)	0.33 (0.31, 0.36)
Kimi-VL-A3B-Instruct	32.11 (31.81, 32.66)	1.65 (1.50, 1.81)	6.62 (6.09, 7.17)	8.60 (7.95, 9.34)
Kimi-VL-A3B-Thinking	34.09 (33.87, 34.24)	0.34 (0.32, 0.36)	1.44 (1.40, 1.49)	1.74 (1.68, 1.78)
Gemma3-27B	36.02 (35.76, 36.34)	0.03 (0.03, 0.03)	0.13 (0.13, 0.13)	0.26 (0.24, 0.29)
MiMo-VL-7B-SFT	35.40 (34.77, 36.34)	0.09 (0.06, 0.11)	0.37 (0.26, 0.48)	0.66 (0.53, 0.73)
MiMo-VL-7B-RL	34.97 (34.48, 35.70)	0.10 (0.09, 0.11)	0.40 (0.37, 0.43)	0.74 (0.66, 0.85)
MiniCPM-V-2_6	33.32 (31.96, 35.45)	1.14 (1.01, 1.21)	5.50 (4.28, 6.52)	6.18 (5.36, 6.81)
MiniCPM-o-2_6	35.29 (34.85, 35.91)	0.24 (0.22, 0.27)	0.74 (0.71, 0.76)	1.15 (1.06, 1.21)
Qwen-Omni-3B	35.03 (34.01, 35.58)	0.14 (0.12, 0.15)	0.87 (0.81, 0.97)	0.73 (0.63, 0.82)
Qwen-Omni-7B	37.45 (37.21, 37.80)	0.26 (0.24, 0.29)	1.06 (0.95, 1.25)	1.24 (1.15, 1.37)
Qwen2.5-VL-7B	37.17 (35.87, 38.82)	4.43 (3.73, 4.83)	15.14 (13.10, 16.53)	13.27 (12.00, 14.01)
Qwen2.5-VL-32B	42.43 (42.04, 42.81)	0.21 (0.20, 0.22)	2.08 (2.00, 2.13)	1.74 (1.70, 1.78)
Qwen2.5-VL-72B	41.89 (41.82, 41.97)	0.24 (0.20, 0.27)	1.62 (1.50, 1.69)	2.37 (2.11, 2.57)
InternVL3-8B	34.77 (34.33, 35.54)	0.98 (0.89, 1.08)	4.37 (4.08, 4.59)	4.35 (4.05, 4.62)
InternVL3-78B	36.70 (36.54, 36.85)	0.16 (0.14, 0.17)	1.39 (1.39, 1.40)	0.92 (0.88, 0.97)
MedVLM-R1	31.25 (30.68, 31.73)	2.42 (2.39, 2.45)	7.66 (7.61, 7.74)	10.85 (10.75, 11.04)
Lingshu-7B	35.41 (34.71, 36.04)	0.71 (0.69, 0.75)	2.74 (2.65, 2.85)	3.02 (2.93, 3.18)
Lingshu-32B	34.69 (34.28, 35.14)	0.11 (0.10, 0.12)	0.59 (0.58, 0.60)	0.74 (0.69, 0.83)
MedGemma-4B	37.09 (36.36, 37.48)	0.05 (0.03, 0.06)	0.32 (0.27, 0.38)	0.58 (0.52, 0.64)
MedGemma-27B	35.98 (34.86, 36.63)	0.05 (0.04, 0.06)	0.24 (0.18, 0.30)	0.44 (0.37, 0.50)
SurgVLM-72B	69.52 (69.21, 69.75)	46.65 (46.34, 46.91)	58.16 (57.83, 58.45)	74.58 (74.16, 74.92)
UniSWM	**65.98 (62.85, 69.85)**	**92.14 (91.55, 92.83)**	**96.98 (96.77, 97.24)**	**93.56 (93.16, 94.16)**

C LARGE LANGUAGE MODELS USAGE STATEMENT

In this study, LLMs were not involved in any content creation. Their use was limited strictly to language polishing. The complete manuscript draft was produced by the authors, with LLMs only used to optimize English grammar and improve the clarity of expression.